Improving Soft Pneumatic Actuator Fingers through Integration of Soft Sensors, Position and Force Control, and Rigid Fingernails

John Morrow[1], Hee-Sup Shin[2], Calder Phillips-Grafflin[1], Sung-Hwan Jang[2], Jacob Torrey[1], Riley Larkins[1], Steven Dang[1], Yong-Lae Park[2], and Dmitry Berenson[1]

***Abstract*— Soft Pneumatic Actuators (SPAs) have recently become popular for use as fingers in robotic hands because of their inherent compliance, low cost, and ease of construction. We seek to overcome two key limitations which limit SPAs' abilities to grasp and manipulate objects: 1) Current SPAs lack position or force sensor feedback, which prevents controlling them precisely (e.g. to achieve a hand preshape or apply a specified pushing force), and 2) the tip of the SPA is compliant and has high friction against common surfaces, causing the SPA to stick against surfaces when grasping objects from above. To overcome the first limitation we propose methods to integrate soft eGaIn sensors into SPAs and controllers that use these sensors' feedback for position and force control. To overcome the second limitation, we explore embedding rigid fingernails into the tip of the SPA so that the finger does not stick against surfaces and can wedge under objects. Our experiments suggest that we can achieve low steady-state error and overshoot in position and force using feed-forward models that relate pressure, force, and curvature along with a PID controller. We also compare several fingernail designs and show that the best-performing design significantly outperforms having no fingernails when grasping a set of common objects from a table.**

I. INTRODUCTION

We seek to develop soft robotic fingers suitable for use in a robotic hand that manipulates common household objects. For instance, the hand should be able to grasp all 27 objects used in the Amazon Picking Challenge (APC) competition [1], as shown in Figure 2, from both flat surfaces (such as a table) and from inside the shelving "pod" used in the APC.

Within this context, we focus on two under-explored areas of soft robotics: first, the integration of sensors and second, the integration of rigid components with soft systems. Grasping objects reliably requires position control to preshape the hand prior to grasping and force control to prevent damaging fragile objects; for both of these aims, the addition of sensors and rigid components has the potential to greatly improve the performance of soft actuators such as the Soft Pneumatic Actuators (SPAs) [2], [3], [4] we use. The integration of sensors within soft actuators enables the use of closed-loop position and force control, whereas most current SPAs rely on open-loop control of the pressure within the actuator to control position and applied force as they lack feedback.

Recent developments of deformable sensors using eGaIn [5] allow integration of sensors that do not impede the compliance of soft actuators. We propose a method to integrate eGaIn-based sensors into SPAs, and develop closed-loop controllers that allow the position and force of our SPAs to be controlled with sufficient accuracy for use in a robot hand.

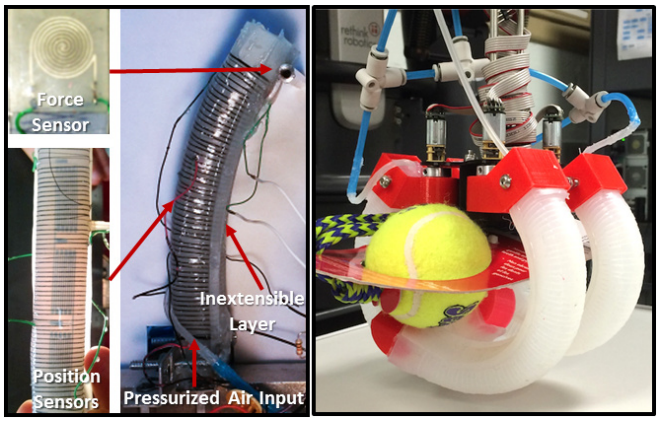

Fig. 1: Left: The components of our SPA, including soft eGaIn sensors. Right: SPAs with our fingernails used as part of a hand.

However, compliance in every part of the SPA is not always desirable. For example, when used for grasping objects from above, the SPA can make contact with the surface the object is resting on. In our experience, this contact often causes the SPA to stick to the surface (due to high friction and compliance) and thus the SPA fails to grasp the object. We propose the use of rigid "fingernails" integrated into the distal end of the SPA to address these issues without compromising the useful compliant behavior of the SPA. We evaluate a series of fingernail designs for use in grasping objects from a table, and show that the best-performing fingernail outperforms the standard SPA in this grasping task.

The contributions of this paper are: 1) Methods to integrate soft position and force sensors with SPAs; 2) Force and position controllers for SPAs with an optional force limit; and 3) Fingernail designs that improve the success rate of grasps from flat surfaces. The rest of this paper details related work, embedding of eGaIn sensors, using embedded sensors for closed-loop control, development and evaluation of fingernail designs, and results showing the efficacy of the controllers and the fingernails.

II. RELATED WORK

SPAs have undergone many changes since their initial development by Galloway et al [2]. Mosadegh et al. designed the PneuNet actuator [3], which uses multiple small air chambers instead of the single chamber design used by Galloway. Deimel and Brock [4] adapted Galloway's actuator to make the PneuFlex actuator, which is the basis for the actuator we use in our work.

[1]Worcester Polytechnic Institute
[2]Carnegie Mellon University

Though SPAs are a popular choice for compliant fingers, alternative compliant hand designs exist. The SDM gripper, featured under-actuated fingers with embedded soft material 'ligaments' to allow compliance [6]. Though the joints of these fingers are compliant, the links are rigid. In this work we seek fingers that can comply to arbitrary geometry and disturbances, so we focus on SPAs. At larger scales, combinations of pneumatic actuators with rigid structural components and sensors have been explored, such as the OctArm manipulators [7].

Precise control of soft actuators is a relatively new field of study, and there has been limited work done on the subject. Most approaches have used the Finite Element Method to control soft systems and have heavy emphasis on modeling the kinematics and dynamics of actuators [8], [9], [10]. Through modeling the dynamics of the pneumatic networks, precise control can be achieved, but it does not take into account the interaction between the actuator and its environment. Also, we seek a real-time controller and solving FEM accurately is not practical in real time. Other approaches attempt to emulate natural behaviors of tentacles and other natural continuum actuators [11]. The approach used in our work takes advantage of having sensors embedded in the actuators, and empirically models the actuator responses.

In this work we use eGaIn sensors developed by Park et al. [5]. These sensors have been applied to a lower limb motion sensing suit which used them to detect gaits [12]. These sensors were also embedded inside fabric [13]. Other types of bending sensors were considered, such as Flexpoint sensors [14]. However, bending sensors must be integrated into the inextensible layer on the inside of the finger, which contacts items being grasped by the hand. Using sensors integrated into the inextensible layer would reduce the compliance of the finger and risk damage to the sensors during grasping, unlike the eGaIn sensors we use, which are mounted on the outside of the finger. Homberg et al [15] have developed a soft gripper similar to ours that integrates bending sensors into SPA-based fingers, however, their sensors are used to identify grasped objects, rather than to provide precise control of the hand.

A key component of our design is the rigid fingernails that can be used to wedge under objects. Loh and Tsukagoshi designed a multi-stage soft actuator to lift the elderly from beds. To get underneath the human, Loh and Tuskagoshi implemented a 'slip-in tip', which is a metal plate that rolls between the body and the bed [16]. The actuator design is similar to ours, however we aim for a passive system to get underneath objects (i.e. a fingernail).

III. Problem Statement

We seek to develop soft robotic fingers for a hand suitable for grasping all 27 objects used in the APC (Figure 2), from both flat surfaces and from inside the bins of the APC shelving "pod". This task requires the ability to preshape the fingers to fit within the confines of the bin (requiring position control), the ability to securely grasp objects without damaging them (requiring force control), and the ability to reliably grasp objects from flat surfaces (requiring fingernails). Specifically, to reach inside the narrowest bin of the shelving pod and grasp the widest object (object 1), we require that the position of the tip of each finger relative to the medial axis of the hand be controllable between 0cm (all fingertips touching) and 10cm (fully open), with error less than 1cm. To securely grasp objects without damaging them, we require that the force exerted by the fingers be controllable such that the most fragile object (object 10) can be grasped (requiring approximately 1N of force) without being crushed (as occurs with more than 2N of force).

Fig. 2: Amazon Picking Challenge objects

IV. Proprioception with Soft Sensors

Typically, the only feedback available from SPAs is the pressure in the actuators, which does not map directly to position or force, due to the well-known non-linear properties of the silicone material. To improve the performance of the actuator through precise force and position control, we use eGaIn sensors, which are deformable and are able to measure the force applied by, and the curvature of, the actuator. The specific circuitry used in the sensing is discussed in [5]. We describe the integration of these sensors below.

A. Force sensing

The grasping force applied by the SPA can be measured using soft eGaIn pressure sensors mounted at the tip. Force applied to the tip of the finger deforms the embedded microchannels filled with eGaIn of the soft sensor, causing an increase in the electrical resistance of the sensor. In this sensor, we chose a spiral microchannel pattern, as shown in Fig. 1, to prevent the sensor from having directional strain sensitivity. The microfluidic soft sensors were individually fabricated using a layered molding and casting process described in [5]. The microchannel pattern was cast into a layer of platinum cure silicone rubber (Dragon Skin-10, Smooth-On), and a thin layer of silicone was adhered atop the microchannels. The eGaIn fluid was then injected using a 25ga hypodermic needle.

B. Position sensing

The position (or shape) of the SPA can be detected using soft eGaIn strain sensors in the SPA structure. Unlike the

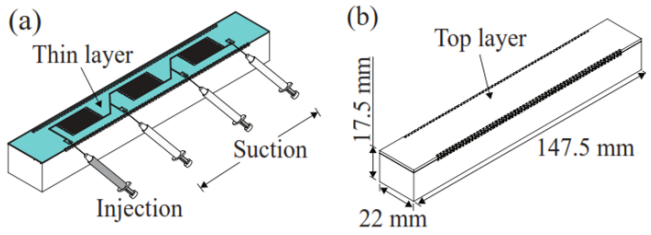

Fig. 3: (a) eGaIn injection process for three soft strain sensors and (b) final assembly of SPA.

force sensors, the strain sensors are directly embedded into dorsal surface of the SPA during fabrication. Since the strain sensors were located off the neutral axis, bending of the finger is easily measured by monitoring the strain changes on the sensors. The SPA contains three strain sensors connected in series, as shown in Figures 1 and 3, each of which consists of a straight serpentine pattern of microchannels to increase sensitivity along the long axis of the finger (in a similar manner as regular strain gauges). These sensors are integrated into the finger by casting the microchannels into the dorsal surface of the SPA. As with the force sensors, the microchannels are covered with a thin layer of silicone, and then eGaIn is injected using a syringe. Since the three sensors are connected in series, the eGaIn for all three sensors can be filled at once, while additional syringes are used to remove air trapped inside the sensors, as shown in Figure 3. The thickness of the actuator walls ensures that the sensor microchannels are not deformed by actuator pressure alone.

V. Mechanical Characterization

Before performing control experiments, the finger prototype was mechanically characterized for both actuation and sensing. The finger was actuated by applying different input pressures up to approximately 138 kPa, and corresponding bending curvatures were measured. The snapshots of the finger bending and the curvature measurement with a standard deviation band are shown in Figure 4. During this actuation, resistance changes of the three position sensors located at the back of the finger were also measured and plotted with curvatures, as shown in the same figure. Although all three sensors provide the same type of information (i.e. curvature), the sensors complement each other. For example, while Sensors 1 and 2 were more sensitive than Sensor 3, Sensor 3 provided a wider dynamic range of sensing. Therefore, by averaging the three sensor signals we can estimate the curvature. One drawback of this method could be increased estimated error levels in a high pressure (or curvature) range, as shown in Figure 5(b).

VI. Force and Position Control

Position and force feedback from the soft sensors enables several forms of closed loop control. The fingertip force sensor allows control of the applied force, while the sensors embedded in the extensible layer of the actuators allow for curvature feedback and thus position control. We implemented three types of controllers using the available sensor

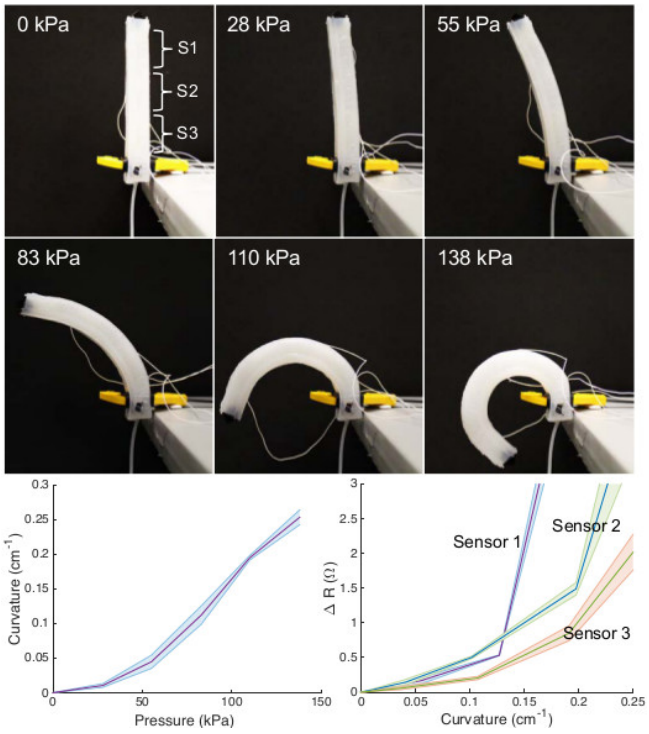

Fig. 4: Mechanical characterization setup and results. Top: Snapshots of finger bending for different input pressure. The top-leftmost figure shows the locations of the three sensors (S1, S2, and S3). Bottom-left: Actuation characterization result for finger bending. Bottom-right: Characterization result of the three position sensors.

feedback: a force controller, a position controller, and a maximum-force position controller. Each controller produces a target pressure, which is then produced by a pressure controller utilizing a pressure transducer for feedback on the actuator pressure (see Figure 6).

All of these controllers are in the form of a PID feedback controller with feed-forward model. Using an accurate feed-forward model reduces the compensation required by the PID control, resulting in improved controller performance. For each finger, a piecewise linear feed-forward model is generated using calibration data collected from the embedded sensors. The piecewise linear feed-forward model is calculated by applying the Ramer-Douglas-Peucker algorithm to the calibration data [17].

A. Pressure Control

Actuator pressure is controlled by a PWM-driven solenoid valve supplied with regulated and filtered compressed air. The PWM signal for the solenoids is commanded by a pressure controller at a frequency of 50 Hz. The pressure controller combines PID feedback (using gains K_p, K_i, K_d) with a piecewise linear feedforward model generated empirically via recording duty cycle D and corresponding actuator pressure. An example calibration curve used to fit the feed-forward model is shown in Figure 5a. The pressure controller equation is shown in Equation 1, with target pressure p_{target}, current measured pressure $p_{current}$, and pressure error $e_p =$

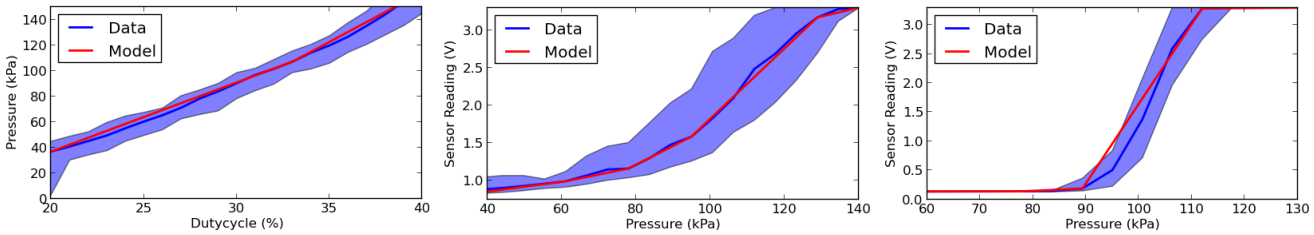

(a) Pressure sensor calibration. (b) Position sensor calibration. (c) Force sensor calibration.

Fig. 5: Calibration curves for the controllers. The red 'model' line is the approximated curve, the blue shaded 'data' area is the range of measured values from multiple trials, and the dark blue 'data' line is the average of the shaded region.

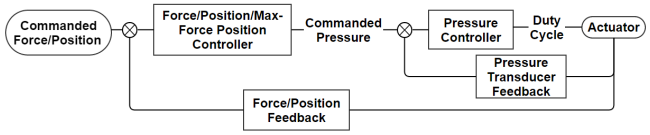

Fig. 6: Controller system block diagram. The force, position, and maximum-force controller outputs are passed into the pressure controller. All the sensors are located on the actuator.

$p_{target} - p_{current}$. The calibrated feedforward model forms the $FF(p_{target})$ term.

$$D = K_{p,p}e_p + K_{i,p}\int e_p dt + K_{d,p}\dot{e}_p + FF(p_{target}) \quad (1)$$

We found that the actuators operate with two different modes of actuation. When increasing the pressure in the actuator, "positive actuation", the maximum rate at which pressure in the actuator can be increased is determined by the external supply pressure. When decreasing the pressure, "negative actuation", the rate at which the pressure is reduced depends on the elasticity of the silicone. As these rates are significantly different, each mode uses its own PID gains.

B. Force Control

For the force controller, the feed-forward term is comprised of a term generated by modeling the force, and a term dependent on the position of the actuator. The position of the actuator contributes a large portion of the feed-forward term, and was introduced to allow the force controller to operate independently of position. The model of the force is generated by observing the relationship between applied force and pressure, and the position term is solely dependent on the actuator position at the time of contact with the object. These relationships and resultant approximations can be seen in Figure 5c. Finding these terms is the second calibration step, which is completed by repeatedly applying forces to an object in the path of the actuator, and recording the force, position, and pressure sensor readings. The position readings are used to compensate for the position at which the force sensor makes contact with the object, isolating the pressure required to apply the force. The pressure to force relationship then yields the force feed-forward term.

The force controller is a PID controller with feedforward terms, as shown in Equation 2. Target pressure is the combination of standard PID feedback in terms of the force error $e_f = f_{target} - f_{current}$ and two feedforward terms. The twin feedforward terms, $FF(f_{target})$ and $FF(x_{current})$, provide the expected actuator pressure for a given target force f_{target} and current finger position $x_{current}$, respectively.

$$p_{target} = K_{p,f}e_f + K_{i,f}\int e_f dt + K_{d,f}\dot{e}_f + FF(f_{target}) + FF(x_{current}) \quad (2)$$

The computed output pressure p_{target} is then used as an input in the pressure controller.

C. Position Control

The position controller incorporates the feedback from the strain sensors embedded in the extensible layer of the actuators. There are three sensors providing feedback, and we assume constant curvature of the actuator (a common assumption in previous work [4]). The three curvature sensor readings are averaged to generate the curvature reading $x_{current}$. The feed-forward term is generated by finding the relation between the averaged curvature sensor reading and pressure. This position feed-forward term is dependent on the desired position of the actuator x_{target}, unlike the term in the force controller that uses the current actuator position. The calibration curves and equations are the same form as those used in the force controller, and are shown in Figure 5b and Equation 3. PID feedback terms are computed in terms of position error $e_x = x_{target} - x_{current}$.

$$p_{target} = K_{p,x}e_x + K_{i,x}\int e_x dt + K_{d,x}\dot{e}_x + FF(x_{target}) \quad (3)$$

D. Maximum-Force Position Control

In the maximum-force position controller, the force feedback and position controller are combined. Controlling the position is the primary function of this controller, but it will limit the force applied by the actuator to ensure the safety of an object in contact with the actuator. When the actuator makes contact with an obstacle, the force feedback will prevent the controller from increasing the actuator force past the specified level, allowing for safe manipulation at any position. As the force feedback approaches the specified threshold $f_{threshold}$, the output of the position controller is attenuated. While the position control signal is being attenuated, a complementary weighting function is applied to the same feed-forward term used in the force controller. This

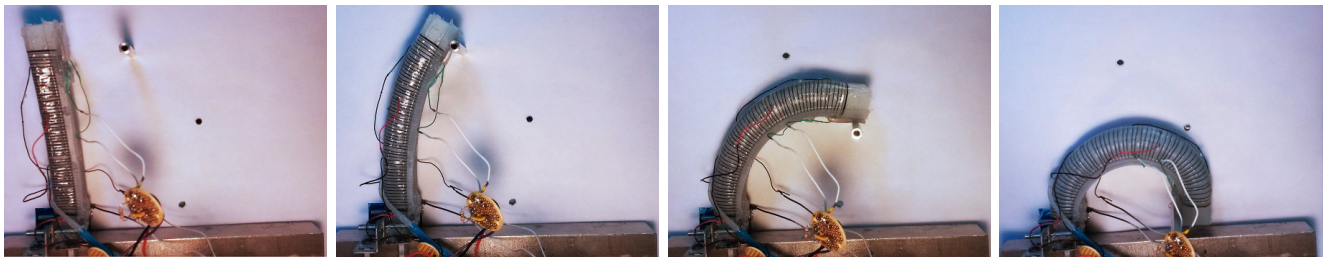

Fig. 7: Actuator at unpressurized position (left-most) and the three obstacle positions (positions 1-3, left to right) used for the force control testing.

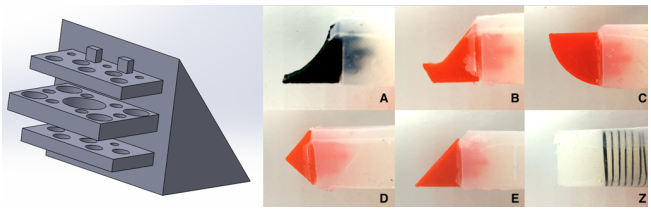

Fig. 8: Left: Anchor design. Right: Set of fingernail designs.

feed-forward term accounts for both position and force, and can sufficiently approximate the necessary pressure to hold the actuator at or below the threshold force. The equation for this controller is shown below.

$$p_{target} = (K_{p,x}e_x + K_{i,x}\int e_x dt + K_{d,x}\dot{e}_x + FF(x_{target}))(1 - e^{-K_g m_f}) + \gamma(FF(x_{current}) + FF(f_{threshold}))(e^{-K_g m_f}) \quad (4)$$

The margin $m_f = f_{threshold} - f_{current}$ term is the difference between the specified force threshold and the current force. The constant K_g was found empirically, and is used to control how rapidly the transition between the position controller and the force control term occurs. The γ is used to account for error in the estimation by scaling the force feed-forward term.

VII. Fingernails

To improve the ability of our soft fingers to grasp objects from flat surfaces, we embed rigid "fingernails" into the tip of each finger. Each fingernail was 3D-printed from ABS plastic and attached during finger fabrication using a porous anchor cast into the tip of the SPA, as shown in Figure 8. We developed a number of candidate fingernail designs, shown in Figure 8, inspired by a range of existing structures. Design A is inspired from the edge of a dustpan, B is inspired from a badger's claws, C is inspired from similar fingertips used by Soft Robotics Inc., D is a simple wedge design, and E is an inclined plane. For comparison, a bare finger is also shown. Evaluation of these candidate fingernail designs is presented in the following section.

VIII. Results

A. Sensor evaluation

To evaluate the accuracy of the integrated eGaIn curvature sensors and ensure that the design requirements were met, we actuated the finger in 1cm steps between 10cm to -1cm w.r.t. the medial axis of the hand. Data was collected from both the onboard eGaIn sensors and an external camera system tracking the tip of the finger, which served as the ground truth. The data collected in this testing can be seen in Figure 9. The fingertip position tracks the setpoint with sub-centimeter error, meeting our requirement for fingertip positioning accuracy. The relationship between measured sensor voltage and fingertip position varies across fingers, but is easily obtainable through calibration. This calibration process consists of a linear regression between the sensor values S and observed fingertip-positions P to produce a linear model in the form of $P = m * S + c$. Using our collected data, we recovered model coefficients $m = -1.145, c = 0.417$ with $R^2 = 0.995$. We applied this model to the recorded sensor data shown in Figure 9, which shows sub-centimeter difference between camera-tracked and sensed fingertip position throughout the finger's range of motion. Note that for the remainder of this paper, finger positions are reported in terms of the measured sensor voltage; however, for any given finger, this calibration process can be performed to map sensor readings to fingertip position.

B. Controller evaluation

The performance of the position and force controllers was measured by observing responses to step and ramp inputs. Testing for the force controller consisted of driving the sensor into a rigid obstacle and measuring the applied force (see the setup in Figure 7). The force controller had different responses depending on the pressure in the actuator, and so was tested at three different positions. Step and ramp responses can be found in Figures 10 and 11; note the relatively fast rise times and low steady-state errors. Rise times for responses in Figure 10(left) were 88ms on average, and the steady state error averaged 5.4% of the step change. The maximum overshoot was 22.8% of the step size, but overshoot only occurred on the final steps of this range of pressures. These numbers were calculated from four trials at position 1, with 10 step inputs for each trial.

The position controller was put through a similar set of tests, with the obstacle to allow the actuator to be unobstructed as it moved through the commanded positions (see Figure 12). The average rise time for the responses in Figure 12(left) was 380ms, the steady state error was 3% of the step size, and the maximum overshoot was 36% of the step size. In general, the position controller was not as susceptible to the hysteresis of the sensors and actuators as the force controller.

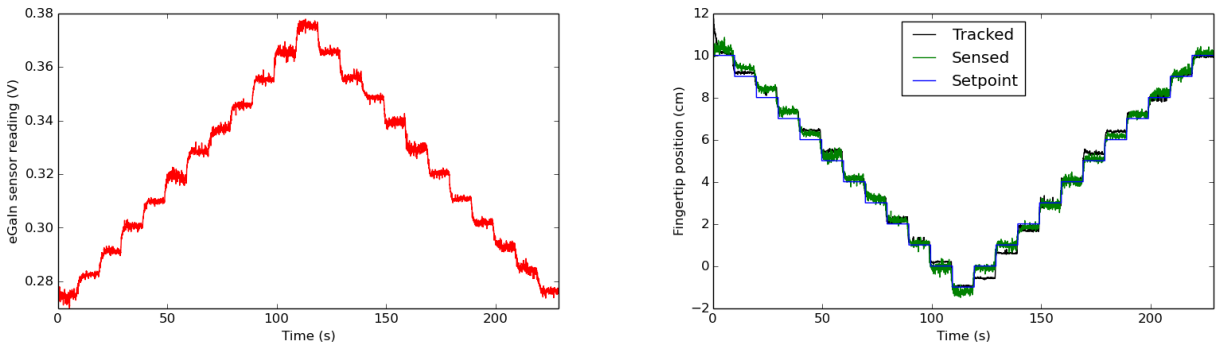

Fig. 9: Evaluation of position control and sensing accuracy using the eGaIn curvature sensors for target positions between 10cm and -1cm of the medial axis of the hand in terms of raw sensor measurements (left) and fingertip position (right). Fingertip position setpoints are shown in blue, positions measured by an external tracking system in black, and position values computed from sensor readings using the calibrated forward model in green.

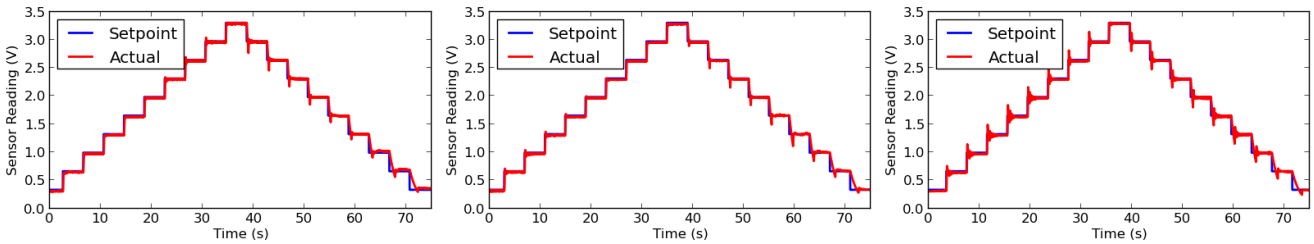

Fig. 10: Force control step responses. Each step is 10% of the total measurable force range. Left-Right: Positions 1-3. Note the increase in overshoot and settling time at Position 3.

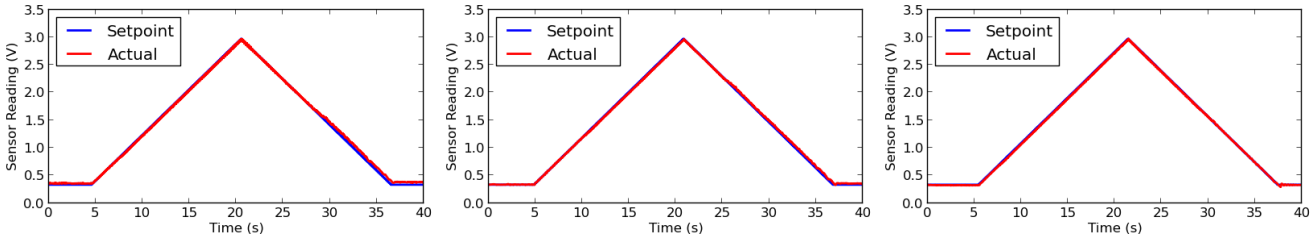

Fig. 11: Force control ramp responses. Left-Right: Positions 1-3.

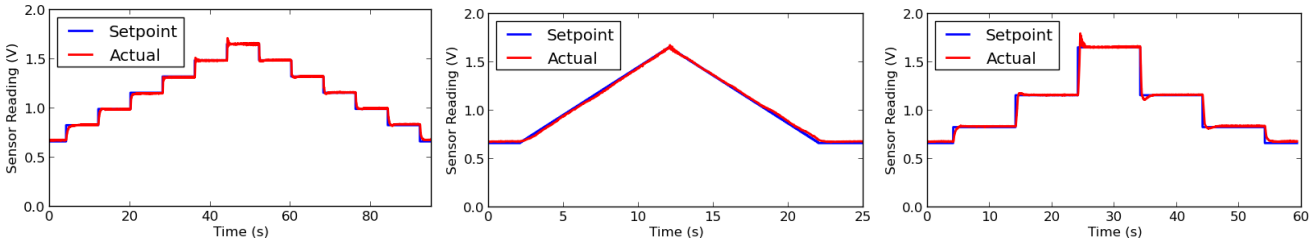

Fig. 12: Position control responses. Left-Right: Positions 1-3.

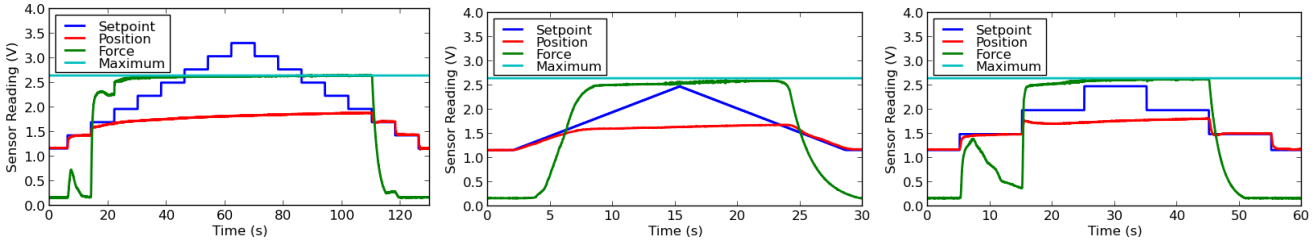

(a) Position controller step responses (b) Position controller ramp response (c) Position controller large step responses

Fig. 13: Maximum-force position control at Position 1. The maximum force was held constant throughout the trials.

For the maximum-force position controller, the same setpoints as for the position controller were used, but the obstacle from the force control tests was put at position 1. In this test, we confirmed that the controller would not drive the actuator past the force threshold. The force threshold was set to an arbitrary force value, with control parameters $\gamma = 0.95$, and $Kg = 6$. For all tests the force remained below the threshold (see Figure 13). Demonstrations of this controller are shown in the attached video.

To test the force requirements of the fingers, the most fragile APC object (object 10) was brought into contact with the finger. Using the maximum-force position controller, it was possible to hold the book, begin to deform the book, and fully deform the book by changing the force threshold values. Holding the book (supporting the book without deforming the pages) required approximately 1N (with a sensor value of 0.99V), beginning to deform the book required 2N (sensor value of 2.3V), and deforming the book required 3N (sensor value of 3.3V). While the force sensor values were not linear with respect to applied force, they provide sufficient resolution to meet our requirement of holding the book without deforming the pages.

For both the force and maximum-force position controllers, the performance of the controller is limited by the response of the force sensor. In our tests, we found the eGaIn soft force sensors to be sensitive to contact geometry; small contact areas could result in higher-than-expected sensor readings because one or more of the microchannels became pinched, while evenly-distributed force across the entire sensor often resulted in lower-than-expected readings as the deformation of the microchannels was limited. While we were still able to meet our requirements despite these limitations, reducing the sensitivity of these sensors to contact geometry is a significant area for future work.

For the testing, the force controller $K_{p,f}$, $K_{i,f}$, and $K_{d,f}$ gains were 80, 90, 0.5 for positive actuation, and 25, 5, and 0.5 for the negative actuation. The position controller $K_{p,x}$, $K_{i,x}$, and $K_{d,x}$ gains were 75, 100, and 0.5 for positive actuation, and 75, 175, and 0.5 for negative actuation. The gains for the pressure controller were 5, 1, and 0.5. These gains were tuned by hand after the calibration process was completed. All controllers were run using a period Δt of 10 ms. For the feed-forward model, the force term only used one line segment, whereas the position and pressure feed-forward terms used four line segments each (see Figure 5).

C. Fingernail evaluation

To evaluate the candidate fingernail designs shown in Figure 8, we tested each design in a practical application using a basic prototype of our 4-finger gripper design (see Figure 1) to evaluate the effectiveness of each fingernail type on grasping the 27 objects used in the APC (shown in Figure 2, ranging from a spark plug to a package of Oreo cookies). In addition to providing further information on which fingernail designs performed better, this test helped confirm that our finger design meets our requirements for a soft hand. Before testing using the entire 4-finger gripper, we performed a series of brief preliminary tests, which indicated that fingernail designs B and E were likely to become stuck on the table surface, and thus these designs were removed from testing.

Bare Finger Results								
1	2	3	4	5	6	7	8	9
10	11	12	13	14	15	16	17	18
19	20	21	22	23	24	25	26	27
Nail A Results								
1	2	3	4	5	6	7	8	9
10	11	12	13	14	15	16	17	18
19	20	21	22	23	24	25	26	27
Nail C Results								
1	2	3	4	5	6	7	8	9
10	11	12	13	14	15	16	17	18
19	20	21	22	23	24	25	26	27
Nail D Results								
1	2	3	4	5	6	7	8	9
10	11	12	13	14	15	16	17	18
19	20	21	22	23	24	25	26	27

TABLE I: Results of testing candidate fingernail designs in a practical application. The colors represent the average success over the trials with green being averages equal to or greater than 80% and red being averages less than 80%.

For each fingernail design, we attempted to grasp every object from a flat table surface. The gripper was mounted to the arm of a Rethink Robotics Baxter robot, and approached the test object from above until the (unpressurized) fingertips were 5cm from the table surface. The four finger actuators were inflated to a constant 22 PSI (sufficient to hold all of the test objects) to grasp the object. Once grasped, the robot raised the gripper and executed a predefined "shaking" trajectory to test the robustness of the grasp. A given trial was successful if the object was held by the hand throughout the test. We conducted five trails for each object; if 4 or more trials succeeded we deemed the object graspable by the hand. Results for all objects are summarized in Table I. Examples of successful and failed grasps are shown in Figure 14.

Using the bare fingers, the gripper was able to grasp 12 of the 27 objects (44%) with at least an 80% success rate. Fingernail design C improved over the bare finger by one more successfully grasped object, resulting in 48.1% of objects grasped. Design A had a better improvement with 59.3% of objects grasped. The most successful design, however, was design D, which allowed the hand to grasp 77.8% of objects. Selected trials from the fingernail tests can be seen in the attached video.

IX. DISCUSSION

Control: While the soft eGaIn sensors we use are sufficient to meet our requirements for position and force control, they suffer from significant hysteresis, as can be observed in the different step responses. When the sensors are deformed or relaxed, the silicone microchannels must change shape, as seen in the work done by Park et al. [5]. The rate of change in microchannel shape determines the response times

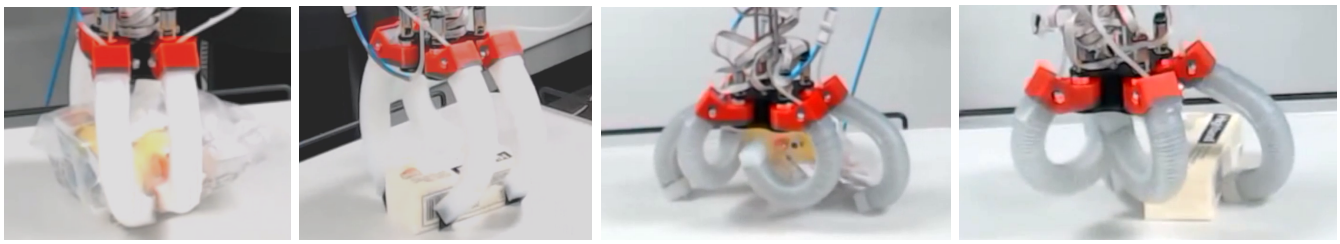

Fig. 14: Examples of fingernail evaluation testing. Using fingernails, as shown in the left two images, objects 22 and 24 are successfully grasped by our prototype hand. However, as shown in the right two images, the bare fingers fail to grasp these objects securely.

of the actuator; in particular, during "negative actuation" the response time is dependent on how quickly the silicone returns to its unpressurized position when the pressure is released. This delay between actuation and sensing can thus result in noticeable overshoot. When used as force sensors, these sensors exhibit considerable sensitivity to contact type and shape. While the contact sensitivity of our force sensors limits their ability to apply precise forces in practice, the sensors provide sufficient feedback to avoid damaging the most fragile of our 27 test items. A major area for future work is to mitigate the contact sensitivity of these eGaIn sensors to enable their use in a broader range of applications.

Fingernails: Fingernail designs A and D were the most successful in testing due to key design features. We believe that the gentle ramp shape of design D provides the best combination of an edge which both helps pick up objects and helps the fingertip slide on the table surface. Designs A and C were both prone to becoming stuck on the table surface, even if the fingernail provided equivalent help in picking up objects. Design A's sharp point was able to get under the items and push the item onto the actuator, while design D's wedge shape guided the item onto the SPA passive layer. As a result, we selected design D for further development of our fingers. While our fingernail designs offered significant improvements in grasp success over the bare finger designs, some objects could not be successfully grasped by any of the nail designs. These objects each offered particular challenges; some require precision grasps for which our prototype hand was poorly suited, while others have slippery surfaces which tend to slip out of the hand. We believe that future development of grasping strategies based on our position and force controllers will improve the success of grasping these objects.

X. CONCLUSION

We have integrated soft eGaIn microfluidic sensors into SPAs to measure the actuator curvature and applied force. Using these embedded sensors to provide feedback, we have developed closed-loop position and force controllers to use our SPAs as fingers in a soft robotic hand. These controllers enable accurate preshaping of the hand prior to grasping, and ensure that objects can be grasped securely without damaging them. In addition, we have explored a series of designs for rigid fingernails integrated into our soft fingers, several of which allow our prototype soft hand design to outperform unmodified fingers in grasping tasks.

XI. ACKNOWLEDGEMENTS

The authors would like to thank Ming Luo, Selim Ozel, and Prof. Cagdas Onal for allowing us to use the equipment in their lab and for their soft robotics advice. This work was supported in part by NSF grants IIS-1551219 and IIS-1524420.

REFERENCES

[1] Amazon, "Amazon Picking Challenge," amazonpickingchallenge.org, 2014.
[2] K. Galloway, P. Polygerinos, C. Walsh, and R. Wood, "Mechanically programmable bend radius for fiber-reinforced soft actuators," in *ICAR*, Nov 2013.
[3] B. Mosadegh, P. Polygerinos, C. Keplinger, S. Wennstedt, R. F. Shepherd, U. Gupta, J. Shim, K. Bertoldi, C. J. Walsh, and G. M. Whitesides, "Pneumatic networks for soft robotics that actuate rapidly," *Advanced Functional Materials*, vol. 24, no. 15, pp. 2163–2170, 2014.
[4] R. Deimel and O. Brock, "A compliant hand based on a novel pneumatic actuator," in *ICRA*, May 2013.
[5] Y.-L. Park, B.-R. Chen, and R. J. Wood, "Design and fabrication of soft artificial skin using embedded microchannels and liquid conductors," *IEEE Sensors Journal*, vol. 12, no. 8, pp. 2711–2718, Aug 2012.
[6] A. Dollar and R. Howe, "A robust compliant grasper via shape deposition manufacturing," *Mechatronics, IEEE/ASME Transactions on*, vol. 11, no. 2, pp. 154–161, April 2006.
[7] M. D. Grissom, V. Chitrakaran, D. Dienno, M. Csencits, M. Pritts, B. Jones, W. McMahan, D. Dawson, C. Rahn, and I. Walker, "Design and experimental testing of the octarm soft robot manipulator," in *Unmanned Systems Technology VIII*, April 2006.
[8] C. Duriez, "Control of elastic soft robots based on real-time finite element method," in *ICRA*, May 2013.
[9] R. Kang, D. T. Branson, T. Zheng, E. Guglielmino, and D. G. Caldwell, "Design, modeling and control of a pneumatically actuated manipulator inspired by biological continuum structures," *Bioinspiration & Biomimetics*, vol. 8, no. 3, p. 036008, 2013.
[10] B. Mosadegh, A. D. Mazzeo, R. F. Shepherd, S. A. Morin, U. Gupta, I. Z. Sani, D. Lai, S. Takayama, and G. M. Whitesides, "Control of soft machines using actuators operated by a braille display," *Lab Chip*, vol. 14, no. 1, pp. 189–199, 2014.
[11] J. Taghia, A. Wilkening, and O. Ivlev, "Position control of soft-robots with rotary-type pneumatic actuators," in *ROBOTIK*, May 2012, pp. 1–6.
[12] Y. Menguc, Y.-L. Park, E. Martinez-Villalpando, P. Aubin, M. Zisook, L. Stirling, R. Wood, and C. Walsh, "Soft wearable motion sensing suit for lower limb biomechanics measurements," in *ICRA*, May 2013.
[13] M. Yuen, A. Cherian, J. Case, J. Seipel, and R. Kramer, "Conformable actuation and sensing with robotic fabric," in *IROS*, Sept 2014.
[14] F. S. Systems, "Flexpoint Bend Sensor," flexpoint.com, 2015.
[15] B. S. Homberg, R. K. Katzschmann, M. R. Dogar, and D. Rus, "Haptic identification of objects using a modular soft robotic gripper," in *IROS*, Sept 2015.
[16] C. Loh and H. Tsukagoshi, "Pneumatic big-hand gripper with slip-in tip aimed for the transfer support of the human body," in *ICRA*, May 2014.
[17] D. H. Douglas and T. K. Peucker, "Algorithms for the reduction of the number of points required to represent a digitized line or its caricature," *Cartographica: The International Journal for Geographic Information and Geovisualization*, vol. 10, no. 2, pp. 112–122, 1973.